ACS APPLIED MATERIALS & INTERFACES

Research Article

www.acsami.org

Graphene Frameworks Promoted Electron Transport in Quantum Dot-Sensitized Solar Cells

Yanyan Zhu,[†,‡] Xin Meng,[†] Huijuan Cui,[†,‡] Suping Jia,*[,†] Jianhui Dong,[†] Jianfeng Zheng,[†] Jianghong Zhao,[†] Zhijian Wang,[†] Li Li,[†] Li Zhang,[†] and Zhenping Zhu*[,†]

[†]State Key Laboratory of Coal Conversion, Institute of Coal Chemistry, Chinese Academy of Sciences, Taoyuan South Road 27, Taiyuan, 030001 China

[‡]University of Chinese Academy of Sciences, Beijing, 100049 China

Supporting Information

ABSTRACT: Graphene frameworks (GFs) were incorporated into TiO_2 photoanode as electron transport medium to improve the photovoltaic performance of quantum dot-sensitized solar cells (QDSSCs) for their excellent conductivity and isotropic framework structure that could permit rapid charge transport. Intensity modulated photocurrent/photovoltage spectroscopy and electrochemical impedance spectroscopy results show that the electron transport time (τ_d) of 1.5 wt % GFs/TiO_2 electrode is one-fifth of that of the TiO_2 electrode, and electron lifetime (τ_n) and diffusion path length (L_n) are thrice those of the TiO_2 electrode. Results also revealed that the GFs/TiO_2 electrode has a shorter electron transport time (τ_d), as well as longer electron lifetime (τ_n) and diffusion path length (L_n), than conventional 2D graphene sheets/TiO_2 electrode, thus indicating that GFs could promote rapid electron transfer in TiO_2 photoanodes. Photocurrent−voltage curves demonstrated that when incorporating 1.5 wt % GFs into TiO_2 photoanode, a maximum power conversion efficiency of 4.2% for QDSSCs could be achieved. This value was higher than that of TiO_2 photoanode and 2D graphene sheets/TiO_2 electrode. In addition, the reasons behind the sensitivity of photoelectric conversion efficiency to the graphene concentration in the TiO_2 were also systematically investigated. Our results provide a basic understanding of how GFs can efficiently promote electron transport in TiO_2-based solar cells.

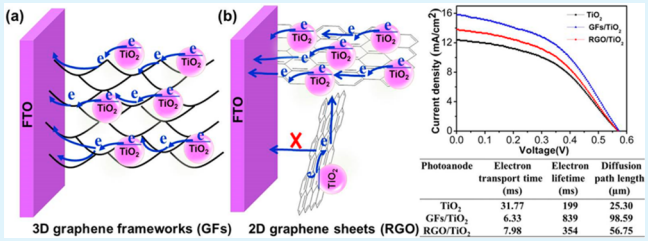

Photoanode	Electron transport time (ms)	Electron lifetime (ms)	Diffusion path length (μm)
TiO_2	31.77	199	25.30
GFs/TiO_2	6.33	839	98.59
RGO/TiO_2	7.98	354	56.75

KEYWORDS: *quantum dot sensitized solar cells, photoanode, graphene frameworks, electron transport, 2D graphene*

1. INTRODUCTION

Quantum dot-sensitized solar cells (QDSSCs), in which quantum dots instead of molecular dyes act as light harvesters, have attracted considerable research interest.[1−7] In QDSSCs, the competition between the transport of electrons through the photoanode and the recombination of electrons with the oxidation state of electrolyte on the electrode−electrolyte interface determines the photoelectrical conversion efficiency (η).[8,9] The conventional photoanode of QDSSCs is composed of TiO_2 nanoparticles with thickness of 10 to 15 μm. These nanoparticles offer a large surface area for sensitizer adsorption. The high porosity is beneficial for the diffusion and storage of electrolyte. However, numerous interparticle boundaries are involved when electron transfer occurs in TiO_2 nanoparticles. These boundaries significantly increase the recombination probability of electrons and holes. Therefore, promotion of photogenerated electron transport in the TiO_2 electrode has become one of the most promising methods by which to improve the photovoltaic performance of cells. Incorporation of conductive nanostructured architectures (such as carbon nanotube and graphene) has been reported as an effective approach to promote electron transport in the TiO_2 photoanode.[10−12] Among these nanostructures, graphene, a two-dimensional single-layer sheet of sp^2 hybridized carbon atoms with exceptional electronic, thermal, and mechanical properties, is extensively used in sensitized solar cells.[12−38] In fabricated TiO_2/graphene composites, graphene could facilitate electron transport in TiO_2 films, thus decreasing the probability of recombination of charge carriers and ultimately improving the photoelectrical conversion efficiency.[12,13,18,27]

Rapid electron transfer occurs within a single graphene nanosheet along its horizontal orientation, whereas the poor electronic contacts between graphene sheets reduce the overall conductivity of the graphene composites because of their anisotropic structure. Particularly at the condensed states similar to the case of electrode, accurately controlling the directional arrangement of the 2D graphene sheet is difficult [shown in Scheme 1a].[39,40] A 2D graphene sheet easily forms irreversible agglomerates because of $\pi-\pi$ interaction, which may also decrease the efficiency of electron transport. However, 3D graphene frameworks (GFs), on account of their excellent conductivity, quasi-isotropic frameworks, and porous structure,

Received: May 25, 2014
Accepted: July 30, 2014
Published: July 30, 2014

Scheme 1. Diagrams of the Photogenerated Electron Transport Route for (a) RGO and (b) GFs Incorporated TiO_2 Photoelectrodes in QDSSCs

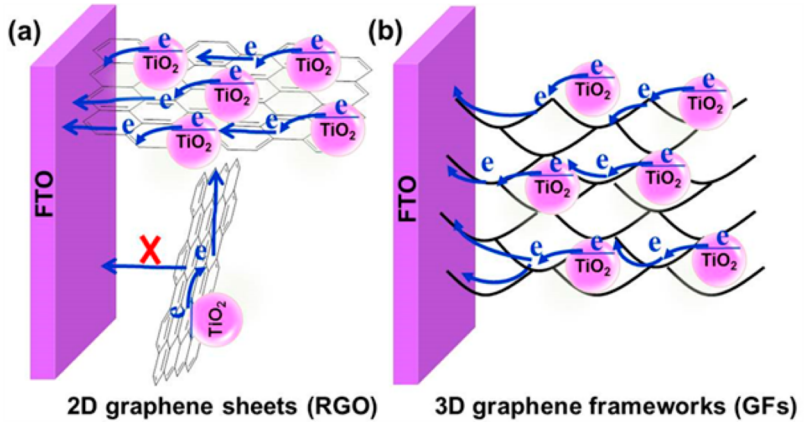

have been studied in numerous energy storage and conversion devices.[41−47] In dye-sensitized solar cells (DSSCs), Tang et al.[40] added the 3D graphene network into the TiO_2 photoanode. The power conversion efficiency increased from 4.96% to 6.58%, which was mainly ascribed to the remarkable electron transport property and considerable specific surface area of the graphene network. However, the application of GFs to QDSSCs has yet to be reported, and the reasons behind the sensitivity of photoelectric conversion efficiency to the graphene concentration in the TiO_2 photoanode remain unclear.

Herein, GFs were constructed through the rapid exfoliation of graphite oxide and incorporated into TiO_2 photoanodes. The quasi-isotropic conductive frameworks could not only prevent the $\pi-\pi$ accumulation of graphene but also provide charge transfer continuity and multiple electron transport channels, as shown in Scheme 1b. These properties are predicted to improve the photoelectric performance of QDSSCs. The effects of GFs on charge transport through the graphene/TiO_2 junction were systematically investigated by intensity-modulated photocurrent/photovoltage spectroscopy (IMPS/IMVS) and electrochemical impedance spectroscopy (EIS) to explain the influence of GFs concentration on the photovoltaic characteristics of GFs incorporated TiO_2-based QDSSCs.

2. EXPERIMENTAL SECTION

2.1. Preparation of GFs and RGO. Graphene oxide (GO) was synthesized by the modified Hummer's method, as described elsewhere.[48] Briefly, graphite powder (3 g) and $NaNO_3$ (1.5 g) were introduced to concentrated H_2SO_4 (18 M, 69 mL) in an ice bath (0 °C), and $KMnO_4$ (9 g) was added gradually while stirring. The mixture was subsequently heated to 35 °C for a 24 h reaction and then diluted with 138 mL of deionized water and further reacted at 98 °C for 15 min. The resulting suspension was further diluted with deionized water to 500 mL, and then, 25 mL of H_2O_2 was added while stirring at room temperature. After washing multiple times with deionized water, the GO was obtained by drying the precipitate of the final slurry at 60 °C for 48 h.

GFs were prepared by subjecting GO to rapid exfoliation under an argon stream according to a previous work.[49] Briefly, the GO powders were placed in a quartz tube with argon stream reflow, and then, the quartz tube was rapidly placed in a tubular furnace that was preheated to a set temperature (e.g., 1000 °C in this work). The quartz tube was taken out of the oven rapidly with a residence time of 30 s. Under this condition, the GO was well exfoliated, controllably reduced, and transformed into GFs.

To compare the properties of the GFs with those of the 2D graphene sheets, chemically reduced graphene oxide (RGO) was also prepared using the previous method by other authors.[50] Typically, GO (100 mg) was dispersed in water (100 mL) and sonicated for 1 h to yield a homogeneous yellow−brown solution. Hydrazine hydrate (1.00 mL, 32.1 mmol) was then added, and the solution was heated at 100 °C for 24 h, and the reduced GO gradually precipitated out as a black solid. This product was filtrated, washed with water thrice, and finally dried at 60 °C.

2.2. Preparation of TiO_2 Films. TiO_2 films were prepared according to a previously reported method.[17] Briefly, certain amounts of graphene were mixed with 4.5 g of TiO_2 (P25 Degussa) directly and stirred evenly to form graphene/TiO_2 slurry. Pure TiO_2 film and graphene/TiO_2 films with different amounts of GFs and RGO (0.1, 0.2, 0.5, 0.8, 1.0, 1.5, and 2.0 wt %) were prepared. Graphene/TiO_2 slurry was then subjected to a spin-coating method on fluorine-doped tin oxide conducting glass (FTO, 14 ohm per square, Nippon Glass Sheet) with an active area of 0.16 cm^2 and then calcined at 450 °C for 30 min under air conditioning. The thickness of the films was controlled by adjusting the rotating time, speed, and the number of rotations [the thickness of the TiO_2 films after calcination was approximately 12 μm (L_d)].

2.3. Fabrication of QDSSCs. The QDSSCs were prepared by referring to previous methods.[51,52] Platinum (Pt) counter electrode was fabricated via thermal decomposition of H_2PtCl_6 on top of FTO. For the QDSSCs photoanodes, chemical bath deposition was used to assemble the QDs on the TiO_2 films. Briefly, CdS was deposited by mixing an aqueous solution of $CdCl_2$ (20 mM), NH_4Cl (66 mM), thiourea (140 mM), and ammonia (230 mM) for about 30 min, subsequently, CdSe was deposited about 5.5 h with the composition of aqueous solution $CdSO_4$ (80 mM), $N(CH_2COONa)_3$ (80 mM) and Na_2SeSO_3(80 mM), both were at 10 °C in the dark. Finally, surface passivation with ZnS was conducted by alternately dipping the photoanodes into 0.1 M $Zn(CH_3COO)_2$ and 0.1 M Na_2S aqueous solution for 1 min and for two cycles. The CdS/CdSe-sensitized TiO_2 photoanode and a Pt-coated FTO counter electrode were assembled to a sandwich-type cell and penetrated with a polysulfide electrolyte that consisted of 2 M Na_2S and 2 M S in methanol, as well as H_2O (v/v = 7:3).

2.4. Characterization Methods. The morphology of GFs, RGO, and graphene/TiO_2 composites films were investigated by field-emission scanning electron microscopy (JSM-7001F, operated at 10 kV) instrument. The atomic force microscope (AFM) image was obtained by using a Nanoscope 4 instrument. Elemental analysis of the products was facilitated by X-ray photoelectron spectroscopy (XPS) (AXIS ULTRA DLD) employing an Al Kα X-ray source. The nitrogen adsorption−desorption isotherms were measured at 77.4 K by using the Micromeritics ASAP 2020 instrument. The photovoltaic properties of the QDSSCs were characterized by recorded photocurrent−voltage ($I-V$) curves using a digital source meter (2400 Source Meter,

Keithley Instruments Inc., U.S.A.) under simulated AM 1.5 illumination (100 mW cm^{-2}) provided by a solar light simulator (San Ei XES-301S). The incident photon-to-current conversion efficiency (IPCE) of the corresponding devices were measured with a Crown instrument over the wavelength range from 300 to 800 nm and with a Si photovoltaic cell as reference. The ultraviolet−visible (UV−vis) absorption spectra of the CdS/CdSe-sensitized photoanode films were measured using a spectrophotometer (UV-3600, Shimadzu, Japan). EIS measurements of the QDSSCs were performed on a Zahner Im6ex potentiostat with frequency range from 0.6 Hz to 100 kHz at an applied bias of $-V_{oc}$ in the dark with AC amplitude of 10 mV. IMPS/IMVS measurements were performed on the same computer-controlled Zahner Im6ex CIMPS potentiostat with a frequency range from 0.6 Hz to 1 kHz and under an intensity of 2 mW cm^{-2} modulated by a blue light-emitting diode (470 nm). The resulting impedance spectra were analyzed with Z-view software.

3. RESULTS AND DISCUSSION

GFs were prepared by the rapid exfoliation and reduction of graphite oxide at 1000 °C for 30 s. The SEM images in Figure 1a evidently display that the GO have been successfully

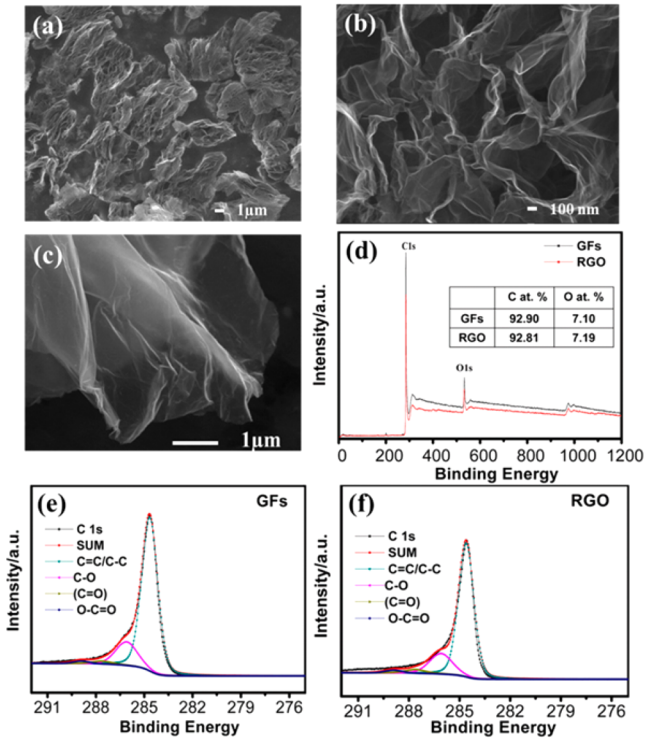

Figure 1. SEM images of GFs (a, b). (c) SEM image of RGO. (d) XPS survey spectra of GFs and RGO. Insets are the relative ratios of carbon and oxygen. (e, f) C 1s XPS profiles of GFs and RGO, respectively.

transformed into 3D frameworks, and Figure 1b shows that GFs are assembled by thin graphene sheets. The obtained GFs are constructed regularly by curved graphene and exhibit large voids in their structures. Supporting Information (SI) Figure S1 displays the AFM image of the thickness of the as-prepared GFs at approximately 1.0 nm, which is in agreement with that cited in previous reports.[49] Figure 1c reveals that the RGO were composed of thin graphene sheets. XPS survey spectra [Figure 1d] revealed the relative ratios of the carbon and oxygen C (92.90 at. %), O (7.10 at. %), and C (92.81 at. %), O (7.19 at. %) for GFs and RGO basically the same. Figure 1e and f show the high-resolution C 1s spectra of GFs and RGO. Four different peaks centered at 284.6, 286.1, 287.6, and 288.9 eV were detected for GFs and RGO, which corresponded to C═C/C−C, C−O, C═O, and O═C−O groups, respectively, and can be well fitted by spectrum deconvolution.[53] The results validate the presence of similar amounts of oxygen-containing groups in the GFs and RGO.

Figure 2a shows the photocurrent−voltage (I−V) characteristic curves of the QDSSCs with different amounts of GFs in

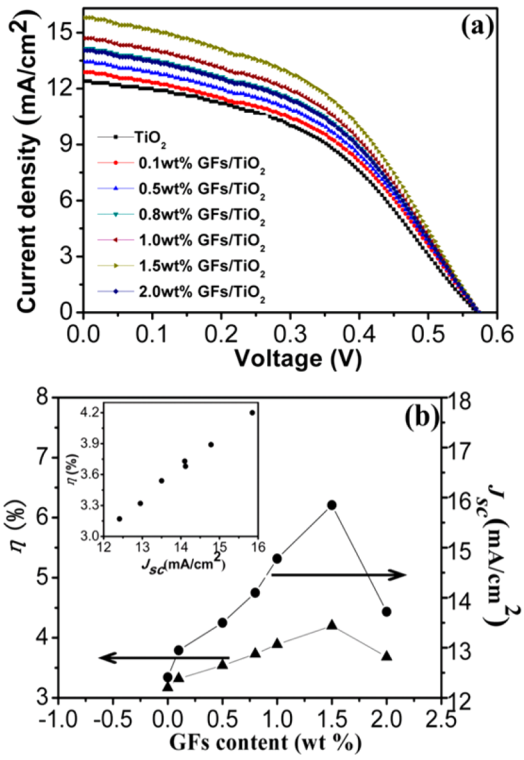

Figure 2. (a) I−V curves of pure TiO_2 and GFs/TiO_2-based QDSSCs vs GFs content, (b) power conversion efficiency (η) and short-circuit current density (J_{sc}) vs GFs content, inset is the relationship of η and J_{sc}.

the TiO_2 photoanodes. Meanwhile, Figure 2b presents the effects of GFs on the photovoltaic parameter power conversion efficiency (η) and short-circuits photocurrent density (J_{sc}) of the cells. As shown in Figure 2b, the η of the QDSSCs increased with GFs content in the low-concentration range and reached the maximum value at 1.5 wt % GFs. However, η decreased when the content of GFs in TiO_2 photoanode further increased because the excessive GFs may act as a recombination center instead of providing electron pathways. Moreover, J_{sc} exhibited a similar trend to η and a linear relationship with η [inset Figure 2b]. Thus, J_{sc} predominantly contributes to the variation in the η value. This phenomenon is consistent with previous reports that incorporated RGO into porous semiconductor photoanodes to facilitate charge transport and improve J_{sc}.[13,18,26] The figures also show that FF and V_{oc} remained almost unchanged throughout the entire GFs concentration range (shown in SI Figure S2). V_{oc} is known to correspond to the difference between the Fermi level in the semiconductor (TiO_2) under illumination and the Nernst potential of the redox couple in the electrolyte.[54] The identical V_{oc} values of the graphene/TiO_2-based cells revealed that the graphene content in the TiO_2 films does not influence the Fermi level of the composite semiconductor. FF is sensitive to the series resistance (R_s).[55,56] R_s remained almost the same after

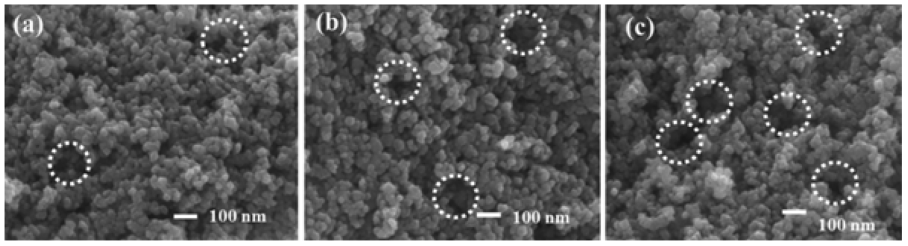

Figure 3. SEM images of (a) pure TiO_2, (b) 1.5 wt % RGO/TiO_2, and (c) 1.5 wt % GFs/TiO_2 photoelectrode films.

incorporating GFs in this study, which is shown in the EIS section.

To validate the superiority of GFs used in the photoanodes, a series of RGO/TiO_2 composite electrodes were fabricated for comparison. *I*−*V* curves (SI Figure S3) display that 1.5 wt % RGO in TiO_2 electrode is also the best one. The amount of GFs in the TiO_2 electrode are very little (1.5 wt %), GFs are almost covered by TiO_2 particles, so the SEM is difficult to distinguish the arrangement of GFs in TiO_2 electrode. We conducted the SEM image for 2.0 wt % GFs/TiO_2 composite electrode, the outlines of GFs exhibit continuous structure and the slightly naked GFs is observed in the TiO_2 electrode shown in SI Figure S4a, b, the TiO_2 nanoparticles fill in the network channels of GFs and cover the outside surface of GFs. Different to the 2.0 wt % GFs/TiO_2 electrode, the outlines of the 2.0 wt % RGO/TiO_2 electrode seems intermittent sheets in SI Figure S4c, d. Figure 3 display the high resolution SEM images of TiO_2, 1.5 wt % RGO/TiO_2, and 1.5 wt % GFs/TiO_2 photoanodes. A rough, coarse morphology of TiO_2/graphene composites electrode films is found in Figure 3, which could improve their ability to adsorb sensitizer.[57] Besides, more large pore can be found in GFs/TiO_2 composites electrode in Figure 3c, indicating that the GFs may as a greater carrier for changing of TiO_2 surface morphology.[39] The large pores are favorable for sensitizer to harvest more photoenergy, meanwhile they can improve the storage and transport of electrolyte molecules in solar cells, which would benefit the cell performance.[38] In addition, the large pores almost do not change the specific surface area of the graphene composites electrodes as investigated by the N_2 adsorption and desorption isotherms SI Figure S5.

I−*V* characteristic curves and detailed photovoltaic parameters of the QDSSCs with TiO_2, 1.5 wt % RGO/TiO_2, and 1.5 wt % GFs/TiO_2 photoanodes are shown in Figure 4a and Table 1. η exhibited considerable improvement to 4.2% for the GFs/TiO_2 photoanode, 33% higher than that of the TiO_2 photoanode, and 17% higher than that of the RGO/TiO_2 electrode. This value suggests that their unique structure makes GFs more conducive than RGO for the transport of electrons in the TiO_2 photoanode. This improvement in the η of QDSSCs is primarily attributed to the increase in J_{sc} as discussed above, which could be reflected in the IPCE performance. Figure 4b shows the IPCE curves for the QDSSCs constructed with three photoanodes. The maximum values of 52%, 59%, and 71% are obtained within a wide range of 400 to 600 nm for pure TiO_2, 1.5 wt % RGO/TiO_2 and 1.5 wt % GFs/TiO_2 photoanodes, respectively, which exhibited a similar trend as J_{sc} in the *I*−*V* curves.

Two factors possibly contribute to the increase in J_{sc} by incorporating graphene into TiO_2 photoanodes:[12,13,18] (1) increasing the amounts of sensitizer absorbed by TiO_2 film, thus increasing the excited electrons from the sensitizer to the conduction band of TiO_2; and (2) promoting the transport of electrons in TiO_2.

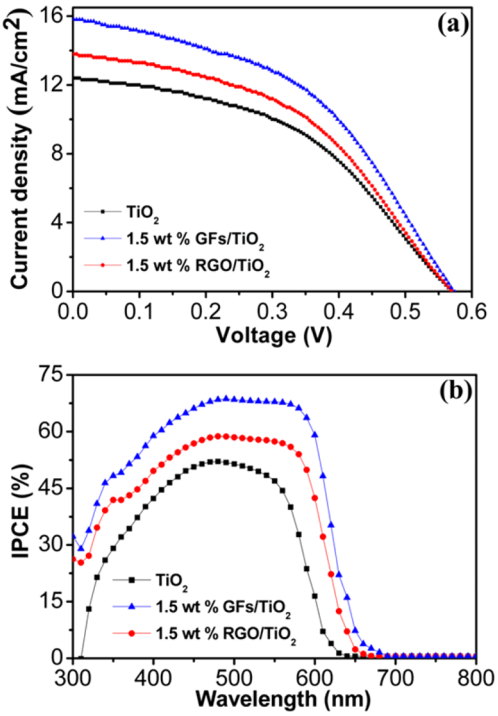

Figure 4. (a) *I*−*V* curves and (b) IPCE spectra of pure TiO_2, 1.5 wt % GFs/TiO_2, and 1.5 wt % RGO/TiO_2-based QDSSCs.

Table 1. Parameters for CdS/CdSe Sensitized Solar Cells Based on the Different Photoanodes

photoanode	J_{sc} (mA/cm^2)	V_{oc} (V)	FF (%)	η (%)
TiO_2	12.41	0.57	44.92	3.17
1.5 wt % GFs/TiO_2	15.89	0.58	45.59	4.20
1.5 wt % RGO/TiO_2	13.70	0.58	45.19	3.58

The UV−vis absorption spectra of three photoanodes show (seen in SI Figure S6, which had been deducted the background of graphene itself absorption) that the absorbance intensity of two complex photoanodes was higher than that of pure TiO_2 photoanode in the range of 400 to 600 nm, which is consistent with other previous reports that incorporated graphene into TiO_2 photoanode to increase sensitizer absorption.[13,18] However, the intensities of 1.5 wt % RGO/TiO_2 photoanode and 1.5 wt % GFs/TiO_2 photoanode are basically identical. Thus, as compared with RGO, the incorporation of GFs in the TiO_2 photoanode does not affect the amounts of QDs in TiO_2 photoanodes. Therefore, GFs could better promote the transport of electrons in TiO_2

photoanode than RGO because of their quasi-isotropic transport frameworks.

IMPS and IMVS have been applied as useful tools in studying electron transport and recombination in solar cells. In this study, the typical IMPS and IMVS values of TiO_2, 1.5 wt % RGO/TiO_2, and 1.5 wt % GFs/TiO_2 photoanodes were measured at a light intensity of 2 mW cm^{-2}, and the characteristic curves and calculated results are shown in Figure 5 and Table 2. The electron transport time (τ_d) and electron

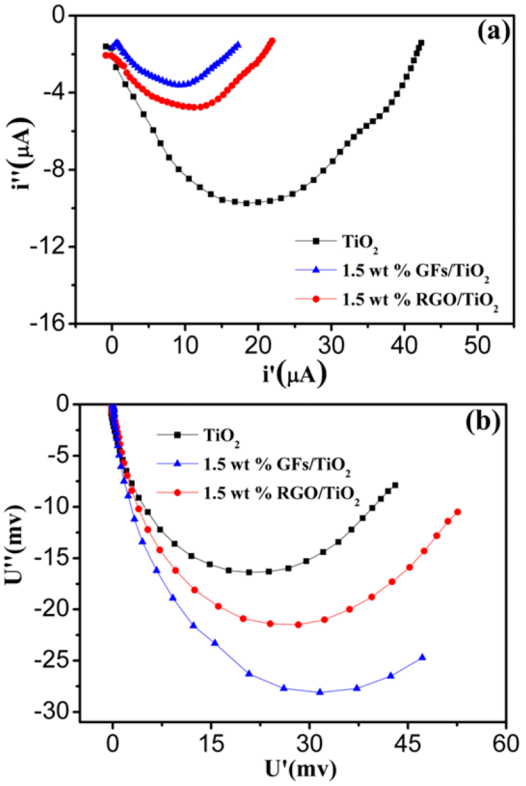

Figure 5. (a) Intensity modulated photocurrent spectroscopy (IMPS) patterns. (b) Intensity modulated photovoltage spectroscopy (IMVS) patterns of pure TiO_2, 1.5 wt % GFs/TiO_2, and 1.5 wt % RGO/TiO_2-based QDSSCs.

lifetime (τ_n) can be calculated by the expressions $\tau_d = 1/2\pi f_{IMPS}$ and $\tau_n = 1/2\pi f_{IMVS}$, similar to those of DSSCs,[58] where f_{IMPS} and f_{IMVS} are the frequency of the minimum IMPS and IMVS imaginary components in Figure 5, respectively. The results shown in Table 2 clearly illustrate that the τ_d of 1.5 wt % GFs/TiO_2-based cells (6.33 ms) is one-fifth of that of the TiO_2 electrode (31.77 ms) and is also shorter than that of 1.5 wt % RGO/TiO_2-based cells (7.98 ms). This observation is related to the considerably faster charge transfer in the GFs/TiO_2-based cells, which results in an enhanced photocurrent compared with that of the RGO/TiO_2-based cells. The electron lifetime (τ_n) derived from the IMVS measurement reflects the recombination processes in QDSSCs. Table 2 shows the τ_n of 1.5 wt % GFs/TiO_2 photoanode (1005 ms) is thrice that of the TiO_2 photoanode (333 ms) and approximately 2-fold larger than that of 1.5 wt % RGO/TiO_2 photoanode (529 ms). Evidently, 1.5 wt % GFs/TiO_2 photoanode showed the longest electron lifetime, reflecting the slowest recombination rate. Therefore, GFs have a shorter τ_d but longer τ_n than RGO, reflecting that GFs could provide more electron paths and promote the faster transport of electrons in TiO_2 photoanodes than RGO.

EIS is further utilized to investigate the interfacial charge transfer and recombination processes of QDSSCs based on the three photoelectrodes. Figure 6 displays the typical Bode and

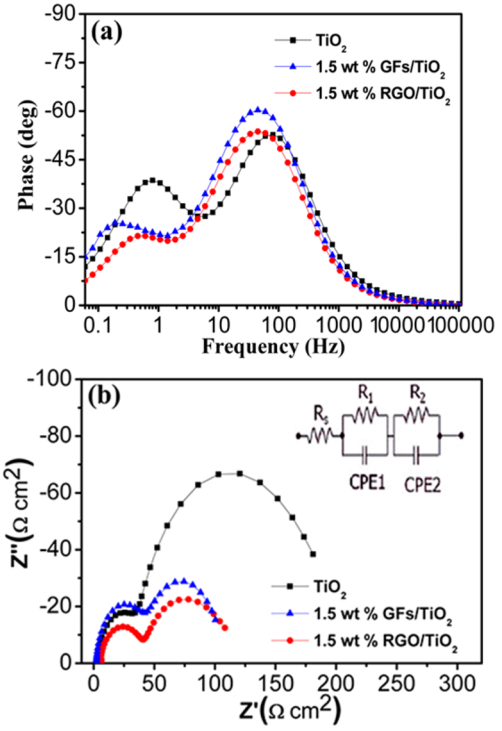

Figure 6. (a) Bode and (b) Nyquist diagrams of electrochemical impedance spectra (EIS) of pure TiO_2, 1.5 wt % GFs/TiO_2, and 1.5 wt % RGO/TiO_2-based QDSSCs.

Nyquist plots of three different photoanodes in QDSSCs at an open circuit bias ($-V_{oc}$) under dark conditions in the frequency range from 0.6 Hz to 100 kHz. As shown in Figure 6a, the characteristic frequency peak for the electron transport process of the GFs and RGO photoanodes shifted to lower frequency compared with pure TiO_2 photoanode. Any shift of the peak from high frequency to low frequency reveals a more rapid electron transport process, because the frequency (f_{mid}) can be related to the inverse of electron lifetime (τ_n) in TiO_2 films as follows:[59] $\tau_n = 1/(2\pi f_{mid})$. The calculated results are shown in Table 2. The electron lifetimes of TiO_2, 1.5 wt % RGO/TiO_2, and 1.5 wt % GFs/TiO_2-based cells were 199, 354, and 839 ms, respectively. As a result, the electron lifetimes of these QDSSCs obtained by EIS showed the same order as the IMVS results,

Table 2. Parameters for CdS/CdSe Sensitized Solar Cells Obtained from EIS, IMPS, and IMVS of Different Photoanodes

photoanode	R_s (Ωcm^2)	R_{ct} (Ωcm^2)	$\tau_{n(bode)}$ (ms)	$\tau_{n(IMVS)}$ (ms)	τ_d (ms)	D_n (10^{-5} cm^2/ s)	L_n (μm)
TiO_2	3.47	142.3	199	333	31.77	1.93	25.30
1.5 wt % GFs/TiO_2	2.25	59.39	839	1005	6.33	9.67	98.59
1.5 wt % RGO/TiO_2	3.83	66.08	354	529	7.98	7.67	56.75

dx.doi.org/10.1021/am503258x | ACS Appl. Mater. Interfaces 2014, 6, 13833−13840

although these values are typically smaller than those obtained from the IMPS, because the EIS measurement was performed in the dark. Therefore, incorporating 1.5 wt % GFs will be more favorable in promoting the transport of electron in TiO_2 photoanodes than RGO. As shown in Figure 6b, the second semicircles at low frequencies describe the charge transport process at the TiO_2 photoanode/electrolyte interface,[3,58,60] which is the crucial factor in the study of photoanodes in devices. The R_{ct} values of the three photoanodes were obtained using Z-view software to fit the semicircles of the midfrequency region. Among the three photoanodes, the 1.5 wt % GFs/TiO_2 photoanode exhibited the smallest R_{ct} at 59.39 Ωcm^2, indicating rapid electron recombination at the photoanode/electrolyte interface, which is unfavorable for the cell performance. This result is in contrast to the above findings.

Combining the above results together showed that GFs can accelerate the electron transfer in photoanodes but simultaneously provides the sites for electron recombination. To identify which effect served the decisive function, different concentration of GFs in TiO_2 photoanodes were analyzed by EIS and IMPS/IMVS, and the test results showed in SI Figure S7. Figure 7a shows the R_{ct} value for each cell with varying GFs

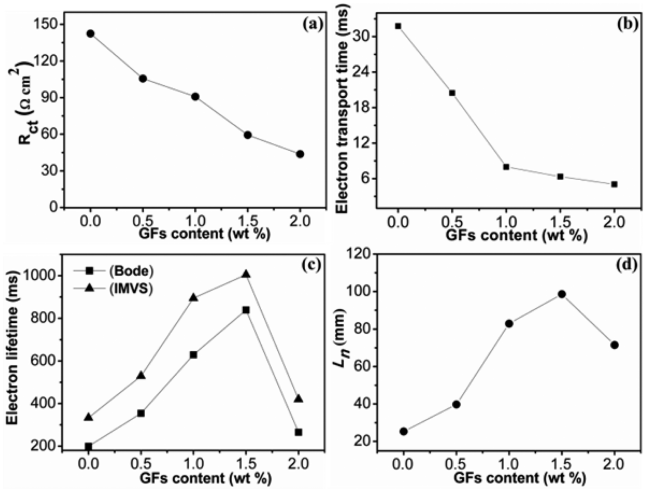

Figure 7. (a) Charge transfer and recombination resistance (R_{ct}), (b) electron transport time (τ_d), (c) electron lifetime (τ_n) obtained from Bode and IMVS, and (d) electron diffusion length (L_n) of pure TiO_2 and GFs/TiO_2-based QDSSCs vs GFs content.

concentrations in the TiO_2 photoanodes. R_{ct} values can be seen to monotonously decrease in the plot, suggesting that charge recombination becomes greater with increasing GFs concentration. The τ_d value for each cell with various GFs concentrations in the TiO_2 photoanodes is shown in Figure 7b. The τ_d values were seen to linearly decrease with increasing GFs concentration, meaning that electron transfer became faster. In addition, Figure 7c shows that in the lower concentration range (less than 1.5 wt %), the τ_n obtained from EIS and IMVS increased with the concentration of GFs but further increased the GFs concentration in the TiO_2 exhibited an undesirable decrease. As graphene is known to possess catalytic activity for the conversion of iodine or sulfide species as catalyst in the counter electrode of DSSCs and QDSSCs.[44,45] Meanwhile, in the photoanode side, excessive graphene cannot to be totally covered by the TiO_2 as SI Figure S4b shown, and direct exposure of the naked graphene to the electrolyte is unavoidable, which means that the recombination of the photogenerated electrons. Subsequently, the incorporation of excessive GFs into the TiO_2 photoanode would result in undesirable electron recombination, explaining why the decrease in η occurred when a higher content of GFs (higher than 1.5 wt %) was incorporated into the TiO_2 photoanode, as mentioned in the $I-V$ section. Competition between electron transport to the conducting substrate and recombination with the S_n^{2-} ions can be expressed by electron diffusion length (L_n), which has a predominant influence on the J_{sc} of the cells. The values of the L_n can be calculated by the expression:[61] $L_n = (D_n\tau_n)^{1/2}$. D_n is the effective diffusion coefficient of electrons in the semiconductor electrode obtained by expression:[61] $D_n = (L_d^2)/(2.35\tau_d)$. Similar to the situation of the J_{sc}, L_n exhibited optimized value at the position of 1.5 wt %, as shown in Figure 7d. The results implied that when incorporating appropriate amounts of GFs in TiO_2 photoanodes, GFs could undertake the role of charge transport channels in the cells and facilitate charge transport in TiO_2 electrodes. However, further increasing the content of GFs in TiO_2 electrode converts GFs instead of as a channel transport of electron but as the center of recombination, accelerate the recombination of electrons and holes, and thus decreasing the J_{sc} and η of the cells.

4. CONCLUSIONS

In conclusion, GFs were successfully used as electron transport medium in TiO_2 photoanodes of QDSSCs. Results showed that when incorporating 1.5 wt % GFs into TiO_2 photoanode, the maximum power conversion efficiency was 4.2% for QDSSCs, which was considerably higher than that of TiO_2 photoanodes and conventional 2D graphene electrodes. In the presence of appropriate amounts of GFs as electron transfer medium in TiO_2 film, photogenerated electrons are scavenged by the GFs and percolate to the collecting FTO electrode, which favors the electron transport through a longer distance with less diffusive hindrance.

■ ASSOCIATED CONTENT

Supporting Information

AFM image of GFs, Figures of V_{oc} and FF vs GFs content, $I-V$ curves, SEM images, N_2 adsorption−desorption isotherms, UV−vis absorption spectra, Nyquist, Bode diagrams of electrochemical impedance spectra (EIS), and intensity modulated photocurrent spectroscopy (IMPS)/intensity modulated photovoltage spectroscopy (IMVS) patterns are presented. This material is available free of charge via the Internet at http://pubs.acs.org.

■ AUTHOR INFORMATION

Corresponding Authors

*Tel: +86-351-4048715. Fax: +86-351-4048433. Email: jiasuping@sxicc.ac.cn.
*Email: zpzhu@sxicc.ac.cn.

Notes

The authors declare no competing financial interest.

■ ACKNOWLEDGMENTS

The authors gratefully acknowledge the financial support from the Natural Science Foundation of China (Nos.51202268), Shanxi Natural Science Foundation (No. 2013011013-4).

REFERENCES

(1) Nozik, A. J. Quantum Dot Solar Cells. *Phys. E* **2002**, *14*, 115−120.
(2) Kamat, P. V. Quantum Dot Solar Cells. Semiconductor Nanocrystals as Light Harvesters. *J. Phys. Chem. C* **2008**, *112*, 18737−18753.
(3) Mora-Seró, I.; Giménez, S.; Fabregat-Santiago, F.; Gómez, R.; Shen, Q.; Toyoda, T.; Bisquert, J. Recombination in Quantum Dot Sensitized Solar Cells. *Acc. Chem. Res.* **2009**, *42*, 1848−1857.
(4) Smith, A. M.; Nie, S. Semiconductor Nanocrystals: Structure, Properties, and Band Gap Engineering. *Acc. Chem. Res.* **2010**, *43*, 190−200.
(5) Rühle, S.; Shalom, M.; Zaban, A. Quantum-Dot-Sensitized Solar Cells. *ChemPhysChem* **2010**, *11*, 2290−2304.
(6) Santra, P. K.; Kamat, P. V. Mn-Doped Quantum Dot Sensitized Solar Cells: A Strategy to Boost Efficiency over 5%. *J. Am. Chem. Soc.* **2012**, *134*, 2508−2511.
(7) Wang, J.; Mora-Seró, I.; Pan, Z. X.; Zhao, K.; Zhang, H.; Feng, Y. Y.; Yang, G.; Zhong, X. H.; Bisquert, J. Core/Shell Colloidal Quantum Dot Exciplex States for the Development of Highly Efficient Quantum-Dot-Sensitized Solar Cells. *J. Am. Chem. Soc.* **2013**, *135*, 15913−15922.
(8) Frank, J. A.; Kopidakis, N.; Lagemaat, J. v. d. Electrons in Nanostructured TiO_2 Solar Cells: Transport, Recombination, and Photovoltaic Properties. *Coord. Chem. Rev.* **2004**, *248*, 1165−1179.
(9) Grätzel, M. Solar Energy Conversion by Dye-Sensitized Photovoltaic Cells. *Inorg. Chem.* **2005**, *44*, 6841−6851.
(10) Kongkanand, A.; Martínez Domínguez, R.; Kamat, P. V. Single Wall Carbon Nanotube Scaffolds for Photoelectrochemical Solar Cells. Capture and Transport of Photogenerated Electrons. *Nano Lett.* **2007**, *7*, 676−680.
(11) Chen, J. Z.; Li, B.; Zheng, J. F.; Zhao, J. H.; Zhu, Z. P. Role of Carbon Nanotubes in Dye-Sensitized TiO_2-Based Solar Cells. *J. Phys. Chem. C* **2012**, *116*, 14848−14856.
(12) Yang, N. L.; Zhai, J.; Wang, D.; Chen, Y. S.; Jiang, L. Two-Dimensional Graphene Bridges Enhanced Photoinduced Charge Transport in Dye-Sensitized Solar Cells. *ACS Nano* **2010**, *4*, 887−894.
(13) Sun, S. R.; Gao, L.; Liu, Y. Q. Enhanced Dye-Sensitized Solar Cell using Graphene−TiO_2 Photoanode Prepared by Heterogeneous Coagulation. *Appl. Phys. Lett.* **2010**, *96*, 083113−083115.
(14) Guo, C. X.; Yang, H. B.; Sheng, Z. M.; Lu, Z. S.; Song, Q. L.; Li, C. M. Layered Graphene/Quantum Dots for Photovoltaic Devices. *Angew. Chem., Int. Ed.* **2010**, *49*, 3014−3017.
(15) He, Z. M.; Guai, G. H.; Liu, J.; Guo, C. X.; Loo, J. S. C.; Li, C. M.; Tan, T. T. Nanostructure Control of Graphene-Composited TiO_2 by a One-Step Solvothermal Approach for High Performance Dye-Sensitized Solar Cells. *Nanoscale* **2011**, *3*, 4613−4616.
(16) Song, J. L.; Yin, Z. Y.; Yang, Z. J.; Amaladass, P.; Wu, S. X.; Ye, J.; Zhao, Y.; Deng, W. Q.; Zhang, H.; Liu, X. W. Enhancement of Photogenerated Electron Transport in Dye-Sensitized Solar Cells with Introduction of a Reduced Graphene Oxide-TiO_2 Junction. *Chem.—Eur. J.* **2011**, *17*, 10832−10837.
(17) Tsai, T. H.; Chiou, S. C.; Chen, S. M. Enhancement of Dye-Sensitized Solar Cells by Using Graphene−TiO_2 Composites as Photoelectrochemical Working Electrode. *Int. J. Electrochem. Sci.* **2011**, *6*, 3333−3343.
(18) Zhu, G.; Xu, T.; Lv, T.; Pan, L.; Zhao, Q. F.; Sun, Z. Graphene-Incorporated Nanocrystalline TiO_2 Films for CdS Quantum Dot-Sensitized Solar Cells. *J. Electroanal. Chem.* **2011**, *650*, 248−251.
(19) Chen, T.; Hu, W. H.; Song, J. L.; Guai, G. H.; Li, C. M. Interface Functionalization of Photoelectrodes with Graphene for High Performance Dye-Sensitized Solar Cells. *Adv. Funct. Mater.* **2012**, *22*, 5245−5250.
(20) Lightcap, I. V.; Kamat, P. V. Fortification of CdSe Quantum Dots with Graphene Oxide. Excited State Interactions and Light Energy Conversion. *J. Am. Chem. Soc.* **2012**, *134*, 7109−7116.
(21) Zhu, P. N.; Nair, A. S.; Pei, S. J.; Yang, S. Y.; Seeram, R. Facile Fabrication of TiO_2−Graphene Composite with Enhanced Photovoltaic and Photocatalytic Properties by Electrospinning. *ACS Appl. Mater. Interfaces* **2012**, *4*, 581−585.
(22) Tang, B.; Hu, G. X. Two Kinds of Graphene-Based Composites for Photoanode Applying in Dye-Sensitized Solar Cell. *J. Power Sources* **2012**, *220*, 95−102.
(23) Wang, H.; Leonard, S. L.; Hu, Y. H. Promoting Effect of Graphene on Dye-Sensitized Solar Cells. *Ind. Eng. Chem. Res.* **2012**, *51*, 10613−10620.
(24) Chen, L.; Zhou, Y.; Tu, W. G.; Li, Z. D.; Bao, C. X.; Dai, H.; Yu, T.; Liu, J. G.; Zou, Z. G. Enhanced Photovoltaic Performance of a Dye-Sensitized Solar Cell Using Graphene−TiO_2 Photoanode Prepared by a Novel In Situ Simultaneous Reduction-Hydrolysis Technique. *Nanoscale* **2013**, *5*, 3481−3485.
(25) Cheng, G.; Akhtar, M. S.; Yang, O. B.; Stadler, F. J. Novel Preparation of Anatase TiO_2@Reduced Graphene Oxide Hybrids for High-Performance Dye-Sensitized Solar Cells. *ACS Appl. Mater. Interfaces* **2013**, *5*, 6635−6642.
(26) Sacco, A.; Porro, S.; Lamberti, A.; Gerosa, M.; Castellino, M.; Chiodoni, A.; Bianco, S. Investigation of Transport and Recombination Properties in Graphene/Titanium Dioxide Nanocomposite for Dye-Sensitized Solar Cell Photoanodes. *Electrochim. Acta* **2013**, *131*, 154−159.
(27) Xu, F.; Chen, J.; Wu, X.; Zhang, Y.; Wang, Y. Y.; Sun, J.; Bi, H. C.; Lei, W.; Ni, Y. R.; Sun, L. T. Graphene Scaffolds Enhanced Photogenerated Electron Transport in ZnO Photoanodes for High-Efficiency Dye-Sensitized Solar Cells. *J. Phys. Chem. C* **2013**, *117*, 8619−8627.
(28) Zhao, J. C.; Wu, J. H.; Yu, F. D.; Zhang, X. P.; Lan, Z.; Lin, J. M. Improving the Photovoltaic Performance of Cadmium Sulfide Quantum Dots-Sensitized Solar Cell by Graphene/Titania Photoanode. *Electrochim. Acta* **2013**, *96*, 110−116.
(29) Chen, L.; Tuo, L.; Rao, J.; Zhou, X. F. TiO_2 Doped with Different Ratios of Graphene and Optimized Application in CdS/CdSe Quantum Dot-Sensitized Solar Cells. *Mater. Lett.* **2014**, *124*, 161−164.
(30) Dai, Y. Q.; Sun, Y. B.; Yao, J.; Ling, D. D.; Wang, Y.; Long, H.; Wang, X. T.; Lin, B. P.; Zeng, T. H.; Sun, Y. M. Graphene-Wrapped TiO_2 Nanofibers with Effective Interfacial Coupling as Ultrafast Electron Transfer Bridges in Novel Photoanodes. *J. Mater. Chem. A* **2014**, *2*, 1060−1067.
(31) He, J. J.; Wu, D. P.; Gao, Z. Y.; Xu, F.; Jiang, S. W.; Zhang, S.; Cao, K.; Guo, Y. M.; Jiang, K. Graphene Sheets Anchored with High Density TiO_2 Nanocrystals and Their Application in Quantum Dot-Sensitized Solar Cells. *RSC Adv.* **2014**, *4*, 2068−2072.
(32) Kim, D.-Y.; Joshi, B. N.; Park, J.-J.; Lee, J.-G.; Cha, Y.-H.; Seong, T.-Y.; In Noh, S.; Ahn, H.-J.; Yoon, S. S. Graphene-Titania Films by Supersonic Kinetic Spraying for Enhanced Performance of Dye-Sensitized Solar Cells. *Ceram. Int.* **2014**, *40*, 11089−11097.
(33) Kusumawati, Y.; Martoprawiro, M.; Pauporté, T. Effects of Graphene in Graphene/TiO_2 Composite Films Applied to Solar Cell Photoelectrode. *J. Phys. Chem. C* **2014**, *118*, 9974−9981.
(34) Liu, Y. L.; Cheng, Y. Q.; Shu, W.; Peng, Z. Y.; Chen, K. Q.; Zhou, J.; Chen, W.; Zakharova, G. S. Formation and Photovoltaic Performance of Few-Layered Graphene-Decorated TiO_2 Nanocrystals Used in Dye-Sensitized Solar Cells. *Nanoscale* **2014**, *6*, 6755−6762.
(35) Zhu, M. H.; Li, X.; Liu, W. W.; Cui, Y. An Investigation on the Photoelectrochemical Properties of Dye-Sensitized Solar Cells Based on Graphene−TiO_2 Composite Photoanodes. *J. Power Sources* **2014**, *262*, 424−428.
(36) Wu, T.-T.; Ting, J.-M. Bridging TiO_2 Nanoparticles Using Graphene for Use in Dye-Sensitized Solar Cells. *Int. J. Energy Res.* **2014**, DOI: 10.1002/er.3162.
(37) Sun, H. C.; Pan, P. K.; Sun, Z. Enhanced Performance of Dye-Sensitized Solar Cells Using Composite Photoanode of TiO_2 Nanofibers, Nanoparticles, and Graphene. *J. Nanosci. Lett.* **2014**, *4*, 25−29.
(38) Fan, J. J.; Liu, S. W.; Yu, J. G. Enhanced Photovoltaic Performance of Dye-Sensitized Solar Cells Based on TiO_2 Nanosheets/Graphene Composite Films. *J. Mater. Chem.* **2012**, *22*, 17027−17036.

(39) Chen, Z. P.; Ren, W. C.; Gao, L. B.; Liu, B. L.; Pei, S. F.; Cheng, H.-M. Three-Dimensional Flexible and Conductive Interconnected Graphene Networks Grown by Chemical Vapor Deposition. *Nat. Mater.* **2011**, *10*, 424−428.
(40) Tang, B.; Hu, G. X.; Gao, H. Y.; Shi, Z. X. Three-Dimensional Graphene Network Assisted High Performance Dye Sensitized Solar Cells. *J. Power Sources* **2013**, *234*, 60−68.
(41) Choi, B. G.; Yang, M. H.; Hong, W. H.; Choi, J. W.; Huh, Y. S. 3D Macroporous Graphene Frameworks for Supercapacitors with High Energy and Power Densities. *ACS Nano* **2012**, *6*, 4020−4028.
(42) Han, S.; Wu, D. Q.; Li, S.; Zhang, F.; Feng, X. L. Porous Graphene Materials for Advanced Electrochemical Energy Storage and Conversion Devices. *Adv. Mater.* **2014**, *26*, 849−64.
(43) Wang, X. B.; Zhang, Y. J.; Zhi, C. Y.; Wang, X.; Tang, D. M.; Xu, Y. B.; Weng, Q. H.; Jiang, X. F.; Mitome, M.; Golberg, D.; Bando, Y. Three-Dimensional Strutted Graphene Grown by Substrate-Free Sugar Blowing for High-Power-Density Supercapacitors. *Nat. Commun.* **2013**, *4*, 2905−2912.
(44) Wang, H.; Sun, K.; Tao, F.; Stacchiola, D. J.; Hu, Y. H. 3D Honeycomb-Like Structured Graphene and Its High Efficiency as a Counter-Electrode Catalyst for Dye-Sensitized Solar Cells. *Angew. Chem., Int. Ed.* **2013**, *52*, 9210−9214.
(45) Ahn, H. S.; Jang, J. W.; Seol, M.; Kim, J. M.; Yun, D. J.; Park, C.; Kim, H.; Youn, D. H.; Kim, J. Y.; Park, G.; Park, S. C.; Kim, J. M.; Yu, D. I.; Yong, K.; Kim, M. H.; Lee, J. S. Self-Assembled Foam-Like Graphene Networks Formed through Nucleate Boiling. *Sci. Rep.* **2013**, *3*, 1396−1403.
(46) Xie, X. Y.; Zhang, C.; Wu, M.-B.; Tao, Y.; Lv, W.; Yang, Q.-H. Porous MnO_2 for Use in a High Performance Supercapacitor: Replication of a 3D Graphene Network as a Reactive Template. *Chem. Commun.* **2013**, *49*, 11092−11094.
(47) Liu, J. J.; Lv, W.; Wei, W.; Zhang, C.; Li, Z. J.; Li, B. H.; Kang, F. Y.; Yang, Q.-H. A Three-Dimensional Graphene Skeleton as a Fast Electron and Ion Transport Network for Electrochemical Applications. *J. Mater. Chem. A* **2014**, *2*, 3031−3037.
(48) Hummers, W. S.; Offeman, R. E. Preparation of Graphitic Oxide. *J. Am. Chem. Soc.* **1958**, *80*, 1339−1339.
(49) Fang, Y.; Luo, B.; Jia, Y. Y.; Li, X. L.; Wang, B.; Song, Q.; Kang, F. Y.; Zhi, L. J. Renewing Functionalized Graphene as Electrodes for High-Performance Supercapacitors. *Adv. Mater.* **2012**, *24*, 6348−6355.
(50) Stankovich, S.; Dikin, D. A.; Piner, R. D.; Kohlhaas, K. A.; Kleinhammes, A.; Jia, Y. Y.; Wu, Y.; Nguyen, S. T.; Ruoff, R. S. Synthesis of Graphene-Based Nanosheets via Chemical Reduction of Exfoliated Graphite Oxide. *Carbon* **2007**, *45*, 1558−1565.
(51) Dong, J. H.; Jia, S. P.; Chen, J. Z.; Li, B.; Zheng, J. F.; Zhao, J. F.; Wang, Z. J.; Zhu, Z. P. Nitrogen-Doped Hollow Carbon Nanoparticles as Efficient Counter Electrodes in Quantum Dot Sensitized Solar Cells. *J. Mater. Chem.* **2012**, *22*, 9745−9750.
(52) Zhang, Q. X.; Guo, X. Z.; Huang, X. M.; Huang, S. Q.; Li, D. M.; Luo, Y. H.; Shen, Q.; Toyoda, T.; Meng, Q. B. Highly Efficient CdS/CdSe-Sensitized Solar Cells Controlled by the Structural Properties of Compact Porous TiO_2 Photoelectrodes. *Phys. Chem. Chem. Phys.* **2011**, *13*, 4659−4667.
(53) László, K.; Tombácz, E.; Josepovits, K. Effect of Activation on the Surface Chemistry of Carbons from Polymer Precursors. *Carbon* **2001**, *39*, 1217−1228.
(54) O'Regan, B.; Gratzel, M. A Low-Cost, High-Efficiency Solar Cell Based on Dye-Sensitized Colloidal TiO_2 Films. *Nature* **1991**, *353*, 737−740.
(55) Han, L.; Koide, N.; Chiba, Y.; Mitate, T. Modeling of an Equivalent Circuit for Dye-Sensitized Solar Cells. *Appl. Phys. Lett.* **2004**, *84*, 2433−2435.
(56) Fabregat-Santiago, F.; Bisquert, J.; Palomares, E.; Otero, L.; Kuang, D.; Zakeeruddin, S. M.; Grätzel, M. Correlation between Photovoltaic Performance and Impedance Spectroscopy of Dye-Sensitized Solar Cells Based on Ionic Liquids. *J. Phys. Chem. C* **2007**, *111*, 6550−6560.
(57) Yen, M.-Y.; Hsiao, M.-C.; Liao, S.-H.; Liu, P.-I.; Tsai, H.-M.; Ma, C. -C. M.; Pu, N.-W.; Ger, M.-D. Preparation of Graphene/Multi-Walled Carbon Nanotube Hybrid and Its Use as Photoanodes of Dye-Sensitized Solar Cells. *Carbon* **2011**, *49*, 3597−3606.
(58) Krüger, J.; Plass, R.; Grätzel, M.; Cameron, P. J.; Peter, L. M. Charge Transport and Back Reaction in Solid-State Dye-Sensitized Solar Cells: A Study Using Intensity-Modulated Photovoltage and Photocurrent Spectroscopy. *J. Phys. Chem. B* **2003**, *107*, 7536−7539.
(59) Kern, R.; Sastrawan, R.; Ferber, J.; Stangl, R.; Luther, J. Modeling and Interpretation of Electrical Impedance Spectra of Dye Solar Cells Operated under Open-Circuit Conditions. *Electrochim. Acta* **2002**, *47*, 4213−4225.
(60) Yu, X.-Y.; Liao, J.-Y.; Qiu, K.-Q.; Kuang, D.-B.; Su, C.-Y. Dynamic Study of Highly Efficient CdS/CdSe Quantum Dot-Sensitized Solar Cells Fabricated by Electrodeposition. *ACS Nano* **2011**, *5*, 9494−9500.
(61) Schlichthörl, G.; Park, N. G.; Frank, A. J. Evaluation of the Charge-Collection Efficiency of Dye-Sensitized Nanocrystalline TiO_2 Solar Cells. *J. Phys. Chem. B* **1999**, *103*, 782−791.